Neuroscience Letters 485 (2010) 65–70

Contents lists available at ScienceDirect

Neuroscience Letters

journal homepage: www.elsevier.com/locate/neulet

A free-radical scavenger protects the neural progenitor cells in the dentate subgranular zone of the hippocampus from cell death after X-irradiation

Kazuya Motomura[a,1], Masatoshi Ogura[a,1], Atsushi Natsume[a,b,*], Hidenori Yokoyama[a], Toshihiko Wakabayashi[a]

[a] Department of Neurosurgery, Nagoya University School of Medicine, Japan
[b] Center for Genetic and Regenerative Medicine, Nagoya University School of Medicine, Japan

ARTICLE INFO

Article history:
Received 9 April 2010
Received in revised form 3 August 2010
Accepted 22 August 2010

Keywords:
Free-radical scavenger
X-irradiation
Neural stem cells
Hippocampus

ABSTRACT

It has been elucidated that cognitive dysfunction following cranial radiotherapy might be linked to the oxidative stress-induced impairment of hippocampal neurogenesis that is mediated by proliferating neural stem or progenitor cells. The novel free-radical scavenger edaravone (3-methyl-1-phenyl-2-pyrazolin-5-one) has been clinically used to reduce neuronal damage following ischemic stroke. Previously, we reported that the free-radical scavenger, edaravone, which is currently used to treat patients with brain ischemia, protected cultured human neural stem cells (NSCs) from radiation-induced cell death; the protective effect was observed more significantly in NSCs than in brain tumor cells. Here, in animal models, we demonstrate that edaravone protects neurons in the subgranular zone (SGZ) of the dentate gyrus of the hippocampus from cell death after irradiation. Moreover, edaravone protected spatial memory retention deficits as determined by Morris water maze tests. Our study may shed some light on the beneficial effects of free-radical scavengers in impaired neurogenesis following cranial radiation therapy.

Cranial radiation therapy is widely used to treat primary and metastatic brain tumors and head and neck cancers. Patients who receive radiotherapy that involves the brain frequently experience a progressive cognitive decline [1,4]. Although white matter necrosis and vasculopathy are overt pathologies caused by radiation-induced injury [15], little is known about the underlying mechanism of learning and memory deficits. Several reports demonstrated the relationship between radiation-induced cognitive dysfunction and apoptosis in hippocampal neurons because of oxidative stress [12,20]. Furthermore, it was reported that ionizing radiation delivered in a single 10 Gy dose of X-rays to the rat brain selectively kills a histomorphologically well-defined population of proliferating cells in the subgranular zone (SGZ) of the dentate gyrus [19]. Other researchers reported that SGZ apoptosis peaked 12 h after irradiation and then continued for 48 h [13]. Moreover, it has been suspected that the newly generated neurons in this region contribute to hippocampal function and that adult hippocampal neurogenesis can be correlated with spatial pattern separation [3].

Previously, we demonstrated that a free-radical scavenger, edaravone, protected human neural stem cells (NSCs) from radiation-induced cell death [11]. Free radicals are highly reactive chemical species and differ from all other species in that they possess an unpaired electron; this electron becomes paramagnetic and relatively reactive [2,5]. It has been observed that free radicals attack polyunsaturated fatty acids of membrane lipids *in vivo*, which results in the oxidative deterioration of membrane lipids; this is known as lipid peroxidation [9,10]. One of the important radiation-induced free-radical species is the hydroxyl radical that indiscriminately attacks neighboring molecules, often at near-diffusion-controlled rates [21]. Hydroxyl radicals are generated by ionizing radiations, either directly by oxidation of water or indirectly by formation of secondary partially reactive oxygen species, including superoxide, hydroxyl, and nitric oxide (NO) radicals. Edaravone interacts biochemically with a wide range of free radicals, donates electrons, and eventually transforms itself to the stable compound, 2-oxo-3-(phenylhydrazono)-butanoic acid (OPB). The agent also exerts pharmacological neuroprotective effects in the case of brain ischemia by decreasing the levels of inducible NO synthase (iNOS) [22,23]. Although edaravone has been reported to inhibit endothelial injury and neuronal damage in brain ischemia, it remains unclear whether it can effectively prevent radiation-induced brain injury. The aim of this study was to investigate whether edaravone can exert protective and anti-apoptotic effects on neurogenesis and cognitive function in mice

* Corresponding author at: Department of Neurosurgery, Nagoya University School of Medicine, 65 Tsurumai-cho, Showa-ku, Nagoya 466-8550, Japan. Tel.: +81 52 744 2353; fax: +81 52 744 2360.
E-mail address: anatsume@med.nagoya-u.ac.jp (A. Natsume).
[1] These authors contributed equally to this study.

0304-3940/$ – see front matter © 2010 Elsevier Ireland Ltd. All rights reserved.
doi:10.1016/j.neulet.2010.08.065

that were irradiated at young age. Our results show that edaravone protects the neurons in SGZ of the dentate gyrus in young mice from radiation-induced cell death.

Male 3-week-old C57BL/J6 mice (SLC, Shizuoka, Japan) were used in all experiments. All experiments were performed in accordance with the Guidelines for Animal Experiments of Nagoya University Graduate School of Medicine.

Edaravone was kindly provided by the Mitsubishi-Tanabe Pharma Corporation (Osaka, Japan). We dissolved 30 mg of edaravone in 500 μl of 1 N NaOH, added 8 ml distilled water, and then adjusted the pH to 7 with 1 N HCl. The final concentration of edaravone was adjusted to 3.0 mg/ml. Mice were irradiated by using an X-ray generator (MBR-1520-3; Hitachi) at 125 kVp and 20 mA, with a filter of 0.5 mm aluminum and 0.2 mm copper. The dose rate was approximately 2.0–2.3 Gy/min. Mice were anesthetized by an intraperitoneal injection of pentobarbital [50 mg/kg body weight (BW)]; sham-irradiated mice (control) were only anesthetized. The cranial X-irradiation beam was directed down onto the head at a source-to-skin distance of 10 cm, while their bodies were shielded with 0.6 mm-thick lead. Mice were housed individually after irradiation in order to minimize the effect of social influences on behavioral tests. Furthermore, mice were injected intraperitoneally with edaravone (3.0 or 6.0 mg/kg BW) 30 min before X-irradiation.

In order to determine the optimal irradiation dose that induces apoptosis in neurons in the SGZ, irradiation of 0, 5, 7.5, or 10 Gy was given to the mouse brain, and brain tissues were collected 48 h later. Sham-irradiated mice were also sacrificed at that time. For tissue collection, mice were deeply anesthetized, and 50 ml of 4% buffered formalin fixative solution was transcardially infused. After 5 min, the brain was removed and immersed in 4% buffered formalin solution for 3 days. Fixed brains were cut coronally at the parieto-occipital junction, thereby providing elongated exposure of each hippocampus.

Apoptosis-positive cells were stained with the MEBSTAIN Apoptosis kit II according to the instructions of the manufacturer (MBL, Nagoya, Japan). We used the anti-neuronal-specific beta-III tubulin antibody (TuJ-1; R&D Systems, Minneapolis, USA) and Alexa Fluor 546 secondary antibodies (Molecular Probes, Eugene, OR, USA) for counterstaining. Following deparaffinization and antigen retrieval using proteinase K, sections were incubated for 30 min in 0.25% Triton X-100/PBS, followed by incubation in 1% gelatin/PBS for 30 min. The sections were washed several times with PBS and incubated at room temperature for 50 min with TuJ-1 (5 μg/ml). Thereafter, the TUNEL reaction mixture was added to the sections and incubated for 10 min at room temperature. The sections were then incubated with the mixture of FITC-dUTP and Alexa Fluor 546 secondary antibodies (1:500) for 1 h in the dark, and then washed with PBS. The number of TUNEL-labeled cells was counted and averaged in bilateral blades in the SGZ. The total number of apoptotic cells was determined by summing the values from all 3 non-overlapping sections for each mouse. All positively labeled cells within the SGZ of the dentate gyrus were quantified by 2 independent observers. The numbers of TUNEL-positive cells were represented as the mean ± SD, and differences among means were evaluated by analysis of variance (ANOVA) (SPSS; SPSS Inc., Chicago, IL, USA). A value of $p < 0.01$ was considered statistically significant.

The novel object recognition test was carried out on 3 consecutive days 48 h after X-irradiation as previously described with slight modifications [7,18]. The apparatus consisted of an open plastic box (30 cm × 30 cm × 30 cm), the outside of which was covered with a black plastic film. The mice were individually habituated in the open box (with no object for 5 min) for 2 days. The mice were tested on the 3rd day. The task consisted of the sample phase and the choice phase. At the start of the sample phase, 2 identical objects (A1 and A2) were placed in the box, 5 cm from the side wall. A mouse was then placed in the box. The total time that the mouse spent exploring the 2 objects was recorded by the experimenter with 2 stopwatches. Exploration of an object was defined as directing the nose to the object at a distance of less than 1 cm and/or touching it with the nose. The mouse was placed back in its home cage after 7 min had elapsed. Fifteen minutes after the sample phase, the mice were reintroduced into the open field for 7 min (choice phase). In this phase, 1 of the familiar objects (A2) was replaced by a new object (B). The time that the mouse spent exploring object B was recorded. The values were represented as percentage time spent for object B of the total time spent for the objects A2 + B.

Morris water maze test was performed as previously described [17]. The circular water tank (60 cm in diameter, 25 cm high) had 4 equally spaced quadrants (north, south, east, and west). First, the mice were trained to locate a visible platform (5 cm in diameter, surface 1 cm above the surface of the water; days 1 and 2), and then a submerged hidden platform (transparent, 5 cm in diameter, surface 2–5 mm below the surface of the water; days 3–5) in 2 daily sessions (3.5 h apart). Each session consisted of 3 trials (60 s each; 10 min intervals). Mice that failed to find the hidden platform within 60 s were placed onto the platform for 15 s. During the training with the visible platform, the platform was moved to a different quadrant in each session. During the training with the hidden platform, the platform was placed in the center of the target quadrant and always kept there for each mouse. The starting point at which the mouse was placed into the water was changed in each trial. The experimenter recorded the time to reach the platform (latency) in each trial. Statistical analysis for behavioral studies was performed using the one-way and two-way analysis of variance (ANOVA) followed by Bonferroni test. A value of $p < 0.05$ was considered statistically significant. Data were expressed as means ± SD.

We determined the optimal radiation dose that induced apoptosis and the timing of observation in the SGZ by exposing 3-week-old mice to various doses (0, 5, 7.5, and 10 Gy) of cranial irradiation. Coronal sections of the brain (including the hippocampus) were analyzed for apoptosis using TUNEL staining. While the number of TUNEL-positive cells observed along the basal layer of the bilateral dentate gyrus (i.e., SGZ) was limited in control group (Fig. 1A, F, 4.8 ± 1.0 cells) and the groups that received 5 Gy (Fig. 1B, F, 11.2 ± 2.8 cells), and 7.5 Gy (Fig. 1C, F, 13.5 ± 2.5 cells), it was significantly increased by 10 Gy-irradiation (Fig. 1D, F, 74.9 ± 3.9 cells, $p < 0.01$). However, we could observe few TUNEL-positive cells at 24 h even after 10 Gy-irradiation (Fig. 1E). Therefore, we concluded that an irradiation dose of 10 Gy induced cell death at 48 h in the SGZ effectively.

In order to assess the effect of edaravone on X-ray-induced apoptosis, mice were treated with edaravone at a final concentration of 0, 3.0, or 6.0 mg/kg BW 30 min prior to X-irradiation. TUNEL staining was performed 48 h after X-irradiation to detect and analyze apoptosis. There was a statistical significance in the difference of TUNEL-positive cells between the group that received only irradiation (Fig. 2A, 74.9 ± 3.9 cells) and the group that received 3.0 mg/kg edaravone (Fig. 2B, 53.6 ± 6.1 cells) ($p < 0.05$). The difference was more dramatic between the group that received only irradiation and the group that received 6.0 mg/kg edaravone (Fig. 2C, 40.6 ± 4.0 cells) ($p < 0.01$). The number of TUNEL-positive cells significantly decreased in the group that received 6.0 mg/kg edaravone (Fig. 2D).

On the basis of these results on the cell injury assessment, a dose of 6.0 mg/kg edaravone was given in two behavioral tests; novel object recognition test and Morris water maze test.

Novel object recognition test was performed to evaluate the hippocampus- and cortex-dependent non-spatial learning and memory (Fig. 3). All mice spent more time exploring the new object (B) than the familiar object (A2), but there was no difference between the groups (in sample phase, control: 48.9 ± 3.0%, irradiated without treatment: 52.3 ± 1.9%, irradiated with treatment of 6 mg/kg of edaravone: 48.3 ± 2.3%, in the choice phase, control:

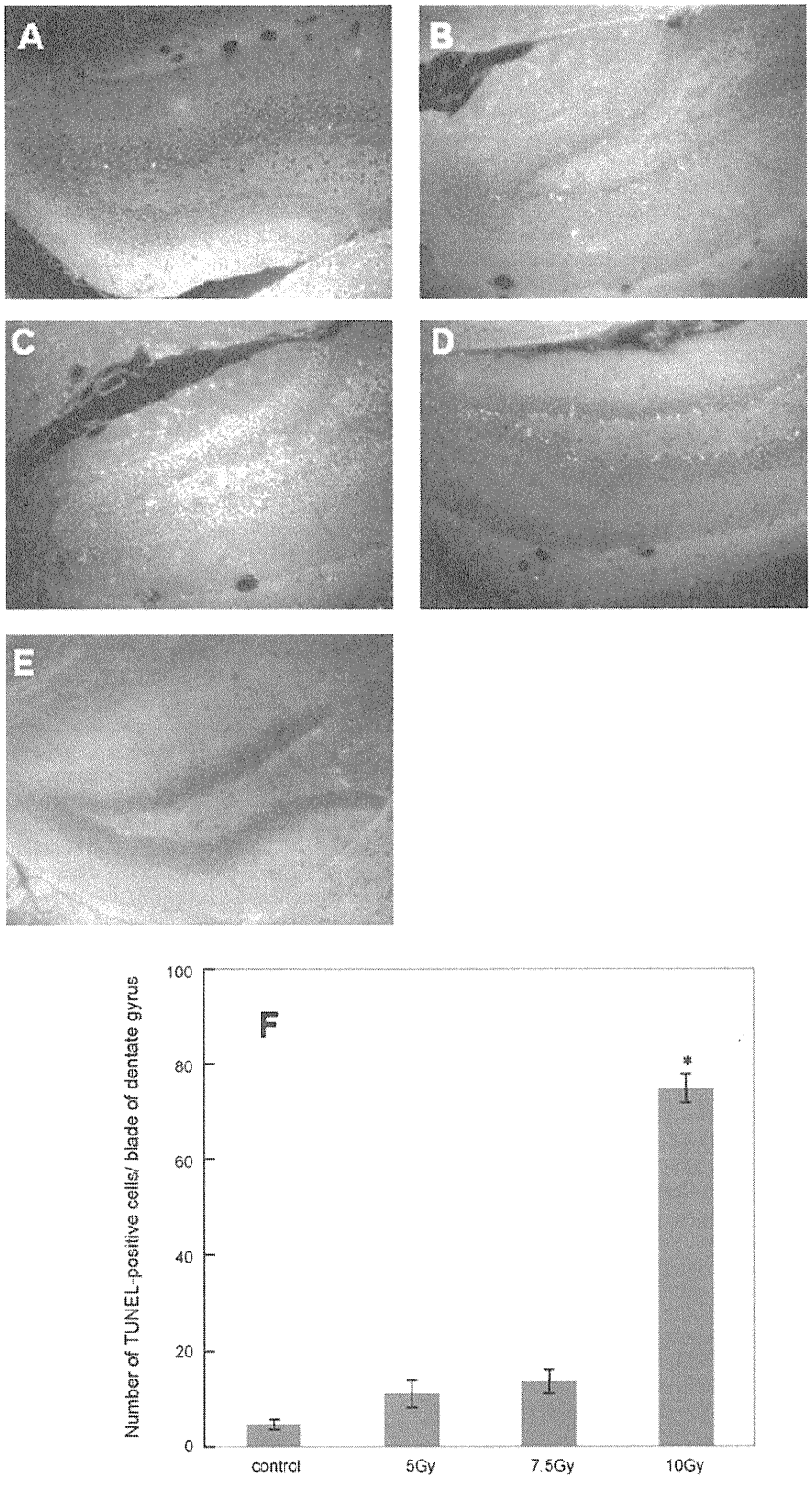

Fig. 1. Double staining of the dentate gyrus of the hippocampus with TUNEL (green) and neuron-specific beta-III tubulin antibody (red) before irradiation (A) and 48 h after X-irradiation with 5 Gy (B), 7.5 Gy (C), 10 Gy (D), and 24 h after 10 Gy-irradiation (E). Occasional TUNEL-positive cells were seen in tissues from non-irradiated mice (control, A). There were no differences between any 2 groups of control, 5, and 7.5 Gy. Compared with those groups, a significant increase of TUNEL-positive cells was seen in the SGZ after irradiation with 10 Gy ($^*p < 0.01$) (F). All micrographs are at 200× magnification. Values are presented as mean ± SEM. The statistical significance of difference was determined by analysis of variance (ANOVA).

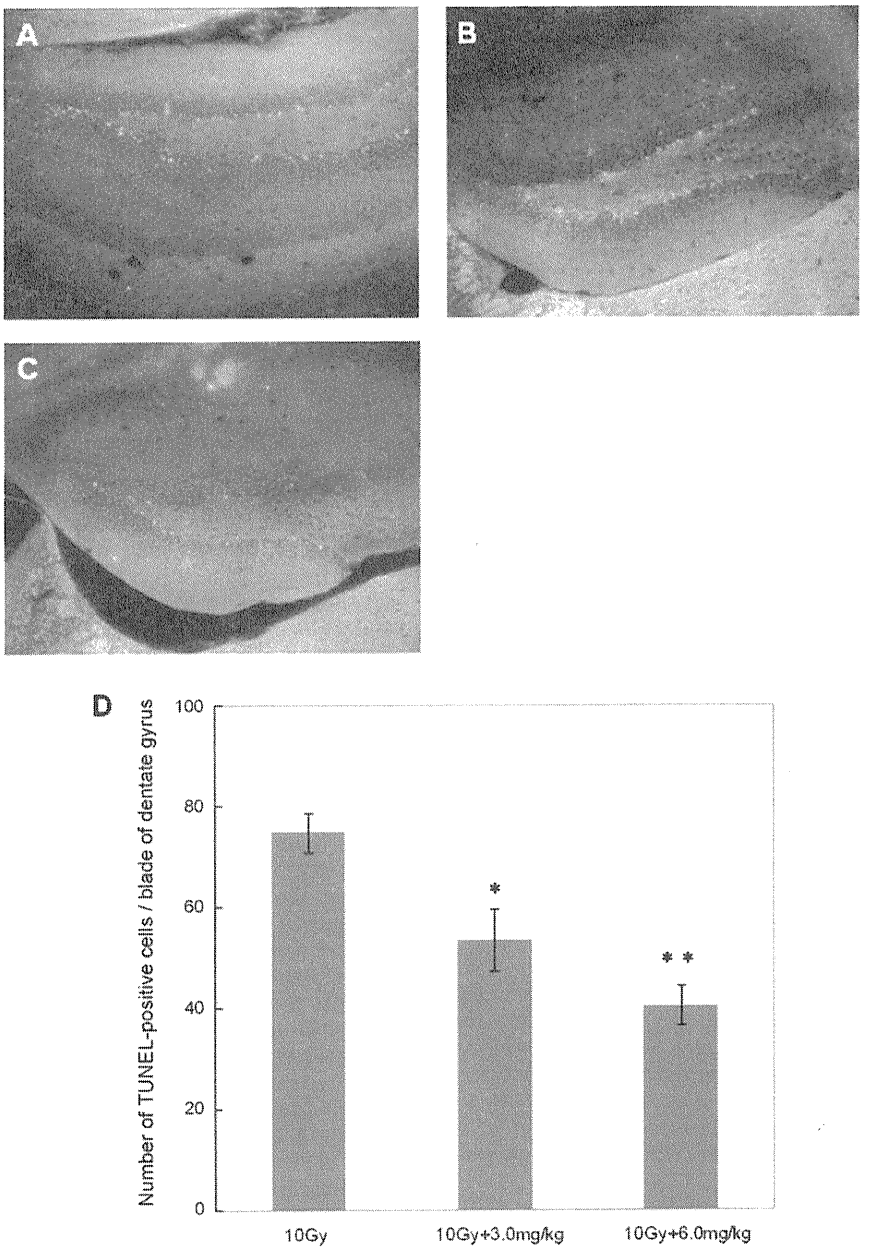

Fig. 2. To assess the effect of edaravone on X-ray-induced apoptosis, mice were treated with edaravone at a final concentration of 0, 3.0, or 6.0 mg/kg BW 30 min prior to X-irradiation. TUNEL staining was performed 48 h after X-irradiation to detect and analyze apoptosis. In the absence of edaravone, there was a significantly higher population of TUNEL-positive cells (A, 74.9 ± 3.9 cells) compared to other groups (B–D). In addition, there was a statistical significance in the difference between the group that received only irradiation and the group that received 3.0 mg/kg edaravone (B and D; 53.6 ± 6.1 cells) ($^{*}p < 0.05$). The difference was more dramatic between the group that was only irradiated and the group that received 6.0 mg/kg edaravone (C and D; 40.6 ± 4.0 cells) ($^{**}p < 0.01$). All micrographs are at 200× magnification. Values are presented as mean ± SEM. The statistical significance of any difference was determined by analysis of variance (ANOVA). Each bar represents an average of 10 mice.

62.9 ± 2.7%, irradiated without treatment: 60.1 ± 3.8%, irradiated with treatment of 6 mg/kg of edaravone: 61.7 ± 2.5%). In addition, we did not observe a difference in the total amount of time that was spent exploring the 2 objects in the sample and choice phase among all groups (in sample phase, control: 26.0 ± 1.5 s, irradiated without treatment: 24.0 ± 1.7 s, irradiated with 6 mg/kg of edaravone: 20.6 ± 1.4 s, in the choice phase, control: 19.4 ± 1.4 s, irradiated without treatment: 21.0 ± 2.1 s, irradiated with 6 mg/kg of edaravone: 19.2 ± 0.9 s). These results suggested that X-irradiation may not affect non-spatial learning and memory among the 3 groups.

In Morris water maze test, all mice improved their performance when the visible (sessions 1–4) and hidden (sessions 5–10) platforms were used. The irradiated mice that received edaravone treatment (6.0 mg/kg) displayed a significantly better learning performance than the untreated mice after irradiation with 10 Gy in sessions 9 and 10 (at session 9, control: 5.23 ± 0.74 s, 10 Gy-irradieted group: 9.09 ± 1.05 s and 10 Gy-irradiated with edaravone injections (6.0 mg/kg) treatment group: 6.65 ± 1.01 s, $p = 0.047$, at session 10, control: 2.06 ± 0.75 s, 10 Gy-irradieted group: 8.99 ± 2.45 s and 10 Gy-irradiated with edaravone injections (6.0 mg/kg) treatment group: 3.75 ± 1.46 s, $p = 0.032$). Data represent means ± SD at sessions 9 and 10 (Fig. 4).

It has recently been understood that radiation-induced cognitive dysfunction might be linked to the impairment of hippocampal

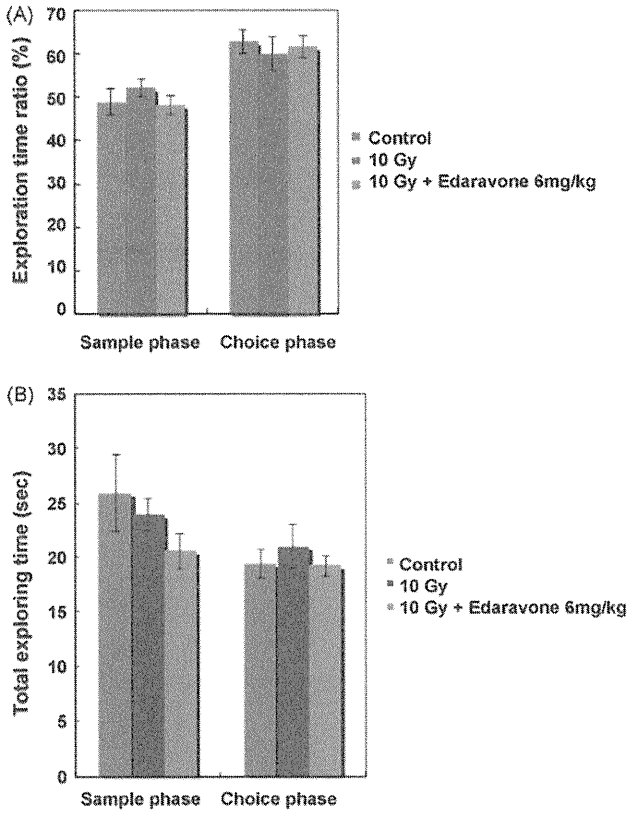

Fig. 3. Novel object recognition test. The exploration time ratio is the time that was spent exploring the new object divided by the total time that was spent exploring the 2 objects. There was no difference in the exploration time ratio and the total amount of time in the sample or choice phase in all groups. Values indicated the means ± SEM. Each bar represents an average of 5 mice.

neurogenesis [15,16]. In the hippocampal region of the central nervous system, neurogenesis continues throughout life. The degree of neurogenesis is closely correlated with the hippocampal functions of memory and learning. Neurogenesis in the hippocampus is mediated by the proliferating neural stem or progenitor cells [8]. In patients who received cranial radiation therapy, the altered microenvironment of the stem cells may hinder essential neurogenesis, thus leading to deficits in learning and memory [14,16].

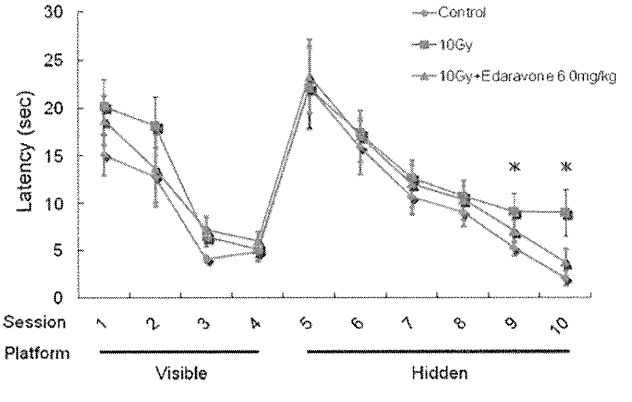

Fig. 4. Water maze performance. Mice were first trained to locate a visible platform (sessions 1–4) and then a submerged hidden platform (sessions 5–10). The time that was needed to reach the platform (latency) was used to quantify the performance. The irradiated mice that received edaravone treatment (6.0 mg/kg) displayed a significantly better learning performance than the untreated mice after irradiation with 10 Gy in sessions 9 and 10 ($^*p < 0.05$). Each bar represents an average of 5 mice. Points and error bar represent mean and standard deviation (SD), respectively.

The present study has extended the results of our previous study by demonstrating that a free-radical scavenger, edaravone, protected human NSCs from radiation-induced cell death. The primary finding of this study in which young mice were used was that neurons in the hippocampus were susceptible to a 10 Gy dose of X-irradiation and that apoptosis was induced. Notably, those apoptotic cells were predominantly observed in the SGZ of the dentate gyrus, presumably among neuronal precursor cells.

Our finding is almost consistent with the fact that neurogenesis in the hippocampus is easily impaired by radiation, although we did not observe apoptosis in the SGZ at 12 h after irradiation, as reported by other studies [13].

Here, we showed that edaravone suppressed X-irradiation-induced apoptosis in neurons in the hippocampus. The clinical therapeutic concentration of edaravone is in concordance with the dose level of 3.0–6.0 mg/kg used in our experiments. These results imply that edaravone can be used as a premedication for cranial radiotherapy. The use of edaravone in premedication should be warranted in a further clinical trial.

Two behavioral tests (i.e., the novel object recognition test and the water maze test) were employed in the present study. The novel object recognition test is based on the natural tendency of mice to investigate a new object instead of a familiar one. The result from this test reflects the learning and recognition memory ability. However, there was no difference in the total amount of time spent on exploring 2 objects in the sample or choice phase in all groups. This test depends on the mood or motivation of the animals, and therefore, it may be difficult to discriminate between control and treated animals. Indeed, few research groups, including even the one which developed this test, reported positive results [6,7]. Unlike the novel object recognition test, the Morris water maze test is widely used to assess the learning and spatial memory in behavioral neuroscience, even though animals are subjected to aversive stimulation to induce a life-threatening escape reaction. This study may indicate the protection of learning and spatial memory in irradiated mice that received edaravone.

In conclusion, we did not address whether edaravone restores neurogenesis in the hippocampus and cognitive function after chronic post-radiation injury. Although further experiments that use animal brain tumor models are required to prove the therapeutic effects, the present study may shed some light on the beneficial effects of free-radical scavengers in impaired neurogenesis following cranial radiotherapy.

Acknowledgments

The authors thank Dr. K. Wakai (Department of Preventive Medicine, Nagoya University) for assisting in the statistical analyses. We also thank Dr. A. Nitta (Department of Neuropsychopharmacology, Nagoya University) for giving us suggestions on behavioral pharmacology.

References

[1] V.A. Anderson, T. Godber, E. Smibert, S. Weiskop, H. Ekert, Cognitive and academic outcome following cranial irradiation and chemotherapy in children: a longitudinal study, Br. J. Cancer 82 (2000) 255–262.
[2] A. Boveris, Biochemistry of free radicals: from electrons to tissues, Medicina (B Aires) 58 (1998) 350–356.
[3] C.D. Clelland, M. Choi, C. Romberg, G.D. Clemenson Jr., A. Fragniere, P. Tyers, S. Jessberger, L.M. Saksida, R.A. Barker, F.H. Gage, T.J. Bussey, A functional role for adult hippocampal neurogenesis in spatial pattern separation, Science 325 (2009) 210–213.
[4] J.R. Crossen, D. Garwood, E. Glatstein, E.A. Neuwelt, Neurobehavioral sequelae of cranial irradiation in adults: a review of radiation-induced encephalopathy, J. Clin. Oncol. 12 (1994) 627–642.

[5] T.L. Dormandy, Free-radical reaction in biological systems, Ann. R. Coll. Surg. Engl. 62 (1980) 188–194.
[6] A. Ennaceur, J. Delacour, A new one-trial test for neurobiological studies of memory in rats. 1. Behavioral data, Behav. Brain Res. 31 (1988) 47–59.
[7] A. Ennaceur, N. Neave, J.P. Aggleton, Neurotoxic lesions of the perirhinal cortex do not mimic the behavioural effects of fornix transection in the rat, Behav. Brain Res. 80 (1996) 9–25.
[8] F.H. Gage, G. Kempermann, T.D. Palmer, D.A. Peterson, J. Ray, Multipotent progenitor cells in the adult dentate gyrus, J. Neurobiol. 36 (1998) 249–266.
[9] B. Halliwell, Role of free radicals in the neurodegenerative diseases: therapeutic implications for antioxidant treatment, Drugs Aging 18 (2001) 685–716.
[10] A.A. Horton, S. Fairhurst, Lipid peroxidation and mechanisms of toxicity, Crit. Rev. Toxicol. 18 (1987) 27–79.
[11] J. Ishii, A. Natsume, T. Wakabayashi, H. Takeuchi, H. Hasegawa, S.U. Kim, J. Yoshida, The free-radical scavenger edaravone restores the differentiation of human neural precursor cells after radiation-induced oxidative stress, Neurosci. Lett. 423 (2007) 225–230.
[12] J.A. Joseph, The putative role of free radicals in the loss of neuronal functioning in senescence, Integr. Physiol. Behav. Sci. 27 (1992) 216–227.
[13] S. Mizumatsu, M.L. Monje, D.R. Morhardt, R. Rola, T.D. Palmer, J.R. Fike, Extreme sensitivity of adult neurogenesis to low doses of X-irradiation, Cancer Res. 63 (2003) 4021–4027.
[14] M.L. Monje, S. Mizumatsu, J.R. Fike, T.D. Palmer, Irradiation induces neural precursor-cell dysfunction, Nat. Med. 8 (2002) 955–962.
[15] M.L. Monje, T. Palmer, Radiation injury and neurogenesis, Curr. Opin. Neurol. 16 (2003) 129–134.
[16] M.L. Monje, H. Toda, T.D. Palmer, Inflammatory blockade restores adult hippocampal neurogenesis, Science 302 (2003) 1760–1765.
[17] R. Morris, Developments of a water-maze procedure for studying spatial learning in the rat, J. Neurosci. Methods 11 (1984) 47–60.
[18] A. Mouri, L.B. Zou, N. Iwata, T.C. Saido, D. Wang, M.W. Wang, Y. Noda, T. Nabeshima, Inhibition of neprilysin by thiorphan (i.c.v.) causes an accumulation of amyloid beta and impairment of learning and memory, Behav. Brain Res. 168 (2006) 83–91.
[19] W. Peissner, M. Kocher, H. Treuer, F. Gillardon, Ionizing radiation-induced apoptosis of proliferating stem cells in the dentate gyrus of the adult rat hippocampus, Brain Res. Mol. Brain Res. 71 (1999) 61–68.
[20] H.F. Poon, V. Calabrese, M. Calvani, D.A. Butterfield, Proteomics analyses of specific protein oxidation and protein expression in aged rat brain and its modulation by L-acetylcarnitine: insights into the mechanisms of action of this proposed therapeutic agent for CNS disorders associated with oxidative stress, Antioxid. Redox Signal. 8 (2006) 381–394.
[21] P.A. Riley, Free radicals in biology: oxidative stress and the effects of ionizing radiation, Int. J. Radiat. Biol. 65 (1994) 27–33.
[22] H. Yoshida, A.H. Kwon, M. Kaibori, K. Tsuji, K. Habara, M. Yamada, Y. Kamiyama, M. Nishizawa, S. Ito, T. Okumura, Edaravone prevents iNOS expression by inhibiting its promoter transactivation and mRNA stability in cytokine-stimulated hepatocytes, Nitric Oxide 18 (2008) 105–112.
[23] N. Zhang, M. Komine-Kobayashi, R. Tanaka, M. Liu, Y. Mizuno, T. Urabe, Edaravone reduces early accumulation of oxidative products and sequential inflammatory responses after transient focal ischemia in mice brain, Stroke 36 (2005) 2220–2225.

J Neurooncol (2010) 98:163–167
DOI 10.1007/s11060-010-0169-x

CLINICAL STUDY/PATIENT STUDY

Gamma knife surgery for 1–10 brain metastases without prophylactic whole-brain radiation therapy: analysis of cases meeting the Japanese prospective multi-institute study (JLGK0901) inclusion criteria

Toru Serizawa · Tatsuo Hirai · Osamu Nagano · Yoshinori Higuchi · Shinji Matsuda · Junichi Ono · Naokatsu Saeki

Received: 6 November 2009 / Accepted: 31 March 2010 / Published online: 22 April 2010

Abstract We evaluated the results of stereotactic radiosurgery (SRS) alone using gamma knife (GK) for selected patients with 1–10 brain metastases without prophylactic whole-brain radiation therapy (WBRT) among JLGK0901-eligible cases. Seven hundred seventy-eight consecutive cases meeting the following JLGK0901 study inclusion criteria were analyzed: (1) newly diagnosed brain metastases, (2) 1–10 brain lesions, (3) less than 10 cm^3 volume of the largest tumor, (4) less than 15 cm^3 total tumor volume, (5) no magnetic resonance (MR) findings of cerebrospinal fluid (CSF) dissemination, and (6) no impaired activity of daily living [<70 Karnofsky Performance Score (KPS)] due to extracranial disease. At initial treatment, all lesions were irradiated with SRS without upfront WBRT. Thereafter, enhanced magnetic resonance imaging (MRI) was applied every 2–3 months, and new distant lesions were appropriately retreated with SRS or WBRT. We divided patients according to tumor number: single lesion for group A (280 cases), 2 for group B (135), 3–4 for group C (148), 5–6 for group D (93), and 7–10 for group E (122). Differences among groups were compared in terms of overall, neurological, qualitative, and new-lesion-free survival (NLFS). Median age was 65 years (range 26–92 years). There were 505 men and 273 women. The primary organ was lung in 579 patients, gastrointestinal tract in 79, breast in 48, urinary tract in 34, and others/unknown in 38. Mean survival time was 0.72 years (0.83 years for 1, 0.69 years for 2, 0.69 years for 3–4, 0.59 years for 5–6, and 0.62 years for 7–10 metastases). On multivariate analysis, significant poor prognostic factors for overall survival (OS) were active systemic disease, poor (<70) initial KPS, and male gender. Neurological survival and qualitative survival at 1 year were 92.7% and 88.2%, respectively. NLFS at 6 months and 1 year were 69.8% and 43.8%, respectively. There were statistically significant differences in new lesion emergence between groups A and B and between groups B and C. SRS using GK provides excellent results in selected patients with 1–10 brain lesions, without prophylactic WBRT. This study revealed that brain lesion number has no effect on any of the four types of survivals, which is anticipated to be confirmed by the JLGK0901 study.

Keywords Metastatic brain tumor · Stereotactic radiosurgery · Gamma knife surgery · Whole-brain radiation therapy · Prospective multi-institute study

T. Serizawa (✉) · T. Hirai
Tokyo Gamma Unit Center, Tsukiji Neurological Clinic, Tokyo, Japan
e-mail: gamma-knife.serizawa@nifty.com

O. Nagano · S. Matsuda · J. Ono
Gamma Knife House, Chiba Cardiovascular Center, Ichihara, Japan

Y. Higuchi · N. Saeki
Department of Neurological Surgery, Chiba University, Chiba, Japan

Introduction

We have treated patients with multiple, even relatively numerous, brain metastases (up to 10 or 25) with stereotactic radiosurgery (SRS) using gamma knife (GK) without prophylactic whole-brain radiation therapy (WBRT) under the same local treatment protocol. We previously reported the effectiveness and limitations of our protocol [5–11]. According to a Japanese randomized controlled study reported by Aoyama et al. [1], the efficacy of SRS alone for 1–4 brain metastases has been established. However,

we GK surgeons have some doubts about this upper limit of only four. Therefore, the Japan Leksell Gamma Knife (JLGK) Society has planned a prospective multi-institute study (Japan Leksell Gamma Knife JLGK0901) for selected patients with 1–10 brain lesions. Herein, we introduce the JLGK study and the anticipated results.

Materials and methods

Among 1,918 patients with metastatic brain tumors treated by GKS from January 1998 through May 2009, 778 who satisfied the following six criteria were analyzed: (1) newly diagnosed brain metastases, (2) 1–10 brain lesions, (3) less than 10 cm^3 volume of the largest tumor, (4) less than 15 cm^3 total tumor volume, (5) no magnetic resonance (MR) findings of cerebrospinal fluid (CSF) dissemination, and (6) no impaired activity of daily living (ADL) (<70 KPS) due to extracranial disease. At initial treatment, all lesions were irradiated with SRS without upfront WBRT. Primary physicians determined chemotherapy protocols. Neurological evaluations and gadolinium-enhanced magnetic resonance imaging (MRI) were performed every 2–3 months at our hospital, or at the primary hospital for as long as possible and then sent to us for evaluation. Dates and causes of death and impaired ADL were documented by the patients' primary physicians. Control of the GKS-treated lesions was defined by absence of any significant increase in tumor diameter (<20%). The applied definitions of "tiny," "small," and "medium" were $\leq$1.0 cm^3, >1.0 but $\leq$4.0 cm^3, and >4.0 but $\leq$10.0 cm^3, respectively. Standard peripheral doses were 22 Gy in tiny, 21 Gy in small, and 20 Gy in medium-sized lesions. We changed the dose by $\pm$2 Gy depending on tumor pathology, physical status, tumor location, extracranial disease status, etc. Neurological death was defined as death due to all forms of intracranial disease, including tumor recurrence, carcinomatous meningitis, cerebral dissemination, and other unrelated intracranial diseases, as described by Patchell et al. [2]. Impaired ADL was defined as impaired neurological status as reflected by KPS <70 (functional preservation), as reported by Aoyama et al. [1]. Intervals from date of SRS treatment until date of death (overall survival, OS), neurological death (neurological survival, NS), impaired ADL (qualitative survival, QS), and appearance of new distant lesions (new-lesion-free survival, NLFS) were calculated by Kaplan–Meier method. We divided patients according to tumor number: single lesion for group A (280 cases), 2 for group B (135), 3–4 for group C (148), 5–6 for group D (93), and 7–10 for group E (122). Differences among groups were compared in terms of OS, NS, QS, and NLFS. A probability value <0.01 was taken to represent a statistically significant difference.

Results

The distributions of patient and treatment factors are summarized in Table 1. Figure 1 shows cumulative tumor-progression-free survival curves according to tumor volume. Tumor control rates at 1 year were 98.4% in tiny, 92.3% in small, and 77.9% in medium-sized tumors. Differences were statistically significant ($p < 0.0001$). The peripheral dose applied to the tumor margin was 13.5–30 Gy [mean $\pm$ standard deviation (SD): 20.7 $\pm$ 1.1 Gy, median: 20 Gy] with a 57.6% isodose contour (range 36–95%). Mean prescribed doses were 21.6 Gy in 281 tiny, 21.1 Gy in 292 small, and 20.1 Gy in 207 medium-sized lesions. Among 70 control-failure lesions, which were clinically diagnosed as tumor recurrence in 38 and radiation injury in 32, surgical removal was required for 9 lesions (7 recurrence, 2 radiation injury).

Mean survival time (MST) was 0.72 years (0.83 years in group A, 0.69 years in group B, 0.69 years in group C, 0.59 years in group D, and 0.62 years in group E), as shown in Fig. 2. MST was 0.83 years in lung cancer, 0.65 years in gastrointestinal (GI) tract, 0.91 years in breast, 0.68 years in urinary tract, and 0.41 in other/unknown origin. There were no significant differences; p values were 0.1596 (A–B),

Table 1 Dichotomized patient characteristics

Characteristics		
Age (years)	Median	65
	Min–max	26–92
Sex	Male	505
	Female	273
Extracranial disease	Controlled	84
	Active	694
Pre-treatment KPS score	Median	100
	Min–max	60–100
Primary organ	Lung	579
	GI tract	79
	Breast	48
	Kidney	34
	Others	38
Number of brain lesions	Median	2
	Min–max	1–10
Maximum lesion volume (cm^3)	Median	1.8
	Min-max	0.1–9.9
Total tumor volume (cm^3)	Median	2.8
	Min–max	0.1–15.0
Metastasis	Synchronous	201
	Metachronous	577
RTOG-RPA classification	Class 1	34
	Class 2	694
	Class 3	50

KPS Karnofsky performance status, *CSF* cerebrospinal fluid

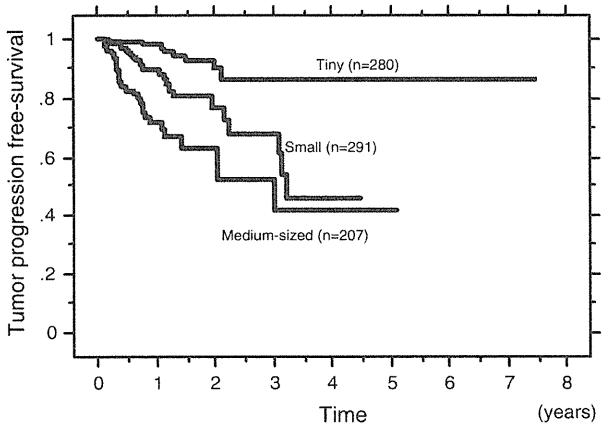

Fig. 1 Tumor-progression-free survival according to tumor volume. The tumor control rate at 1 year was 98.4% for tiny, 92.3% for small, and 77.9% for medium-sized tumors. Differences were statistically significant ($p < 0.0001$). The peripheral dose applied to the tumor margin was 13.5–30 Gy (mean ± SD: 20.7 ± 1.1 Gy, median: 20 Gy) with a 57.6% isodose contour (range 36–95%). Mean prescribed doses were 21.6 Gy in 281 tiny, 21.1 Gy in 292 small, and 20.1 Gy in 207 medium-sized lesions

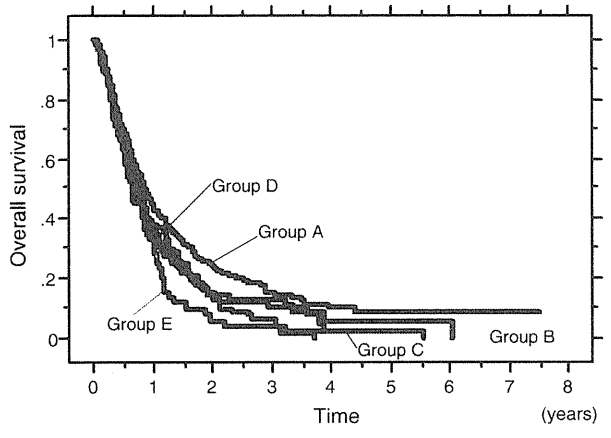

Fig. 2 Overall survival curves according to tumor number. Mean survival time (MST) was 0.72 years (0.83 years in group A, 0.69 years in group B, 0.69 years in group C, 0.59 years in group D, and 0.62 years in group E). There were no significant differences between any two groups; p values were 0.1596 (A–B), 0.2924 (B–C), 0.1594 (C–D), and 0.1050 (D–E)

0.2924 (B–C), 0.1594 (C–D), and 0.1050 (D–E), as shown in Table 2. On multivariate analysis, significant prognostic factors for OS were active extracranial disease [$p < 0.0001$, hazard ratio (HR) 2.994], low pretreatment KPS ($p = 0.0059$, HR 1.517), and male gender ($p < 0.0001$, HR 1.411). Overall survival curves are compared according to Radiation Therapy Oncology Group recursive partitioning analysis (RTOG-RPA) classes, as in Gasper's report [3], in Fig. 3. Mean survival periods were 2.2 years in class 1 ($n = 34$), 0.7 years in class 2 ($n = 694$), and 0.3 years in class 3 ($n = 50$). The differences among groups were statistically significant. Chemotherapy after SRS did not affect overall survival.

Table 2 p Values between pairs of groups

	A vs. B	B vs. C	C vs. D	D vs. E	C vs. E
OS	0.1596	0.2924	0.1594	0.1050	0.8073
NS	0.3860	0.0470	0.5162	0.8454	0.4816
QS	0.7606	0.0163	0.8184	0.6818	0.4142
NLSF	**0.0003**	**0.0047**	0.2905	0.0304	0.2061

Bold values represent statistically significant ($P < 0.01$)

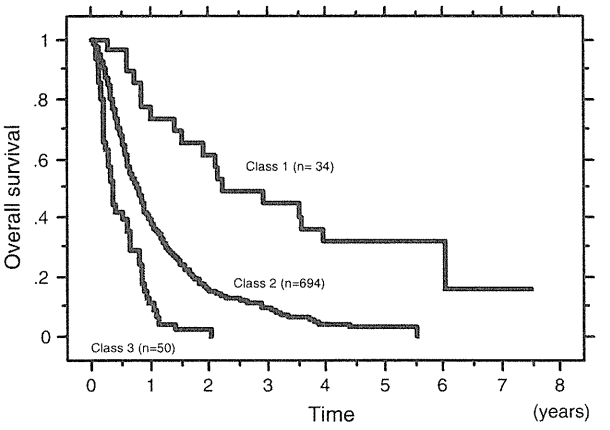

Fig. 3 Overall survival curves according to Radiation Therapy Oncology Group recursive partitioning analysis (RTOG-RPA) class. Mean survival was 2.2 years in class 1 ($n = 34$), 0.7 years in class 2 ($n = 694$), and 0.3 years in class 3 ($n = 50$). The differences among groups were statistically significant ($p < 0.0001$)

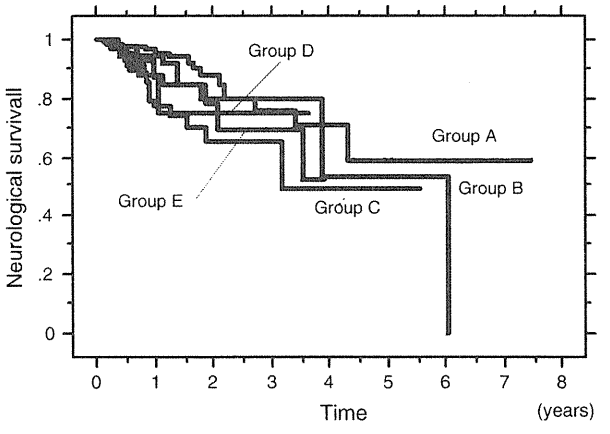

Fig. 4 Neurological survival curves according to tumor number. The neurological survival rate at 1 year was 96.8% in group A, 95.5% in group B, 84.7% in group C, 91.2% in group D, and 89.2% in group E. There were no significant differences between any two sequential groups

The neurological-death-free rate was 92.4% at 1 year and 82.5% at 2 years. Figure 4 shows NS curves according

to tumor number. The NS rate at 1 year was 96.8% in group A, 95.5% in group B, 84.7% in group C, 91.2% in group D, and 89.2% in group E. There were no significant differences between any two adjacent groups (Table 2). Functional-preservation-free survival curves are shown in Fig. 5. The QS rate was 87.8% at 1 year and 73.0% at 2 years in all cases. The functional-preservation-free rate at 1 year was 90.7% in group A, 93.3% in group B, 80.8% in group C, 84.3% in group D, and 85.8% in group E. There were no significant differences between any two sequential groups (Table 2). NLFS curves according to number of brain metastases are shown in Fig. 6. The new-distant-lesion-free rate at 1 year was 54.3%. The new-distant-lesion-free rate at 1 year was 71.6% in group A, 53.7% in group B, 43.6% in group C, 50.7% in group D, and 66.3% in group E. There were significant differences between groups A and B ($p = 0.0003$) and between groups B and C ($p = 0.0047$), as shown in Table 2.

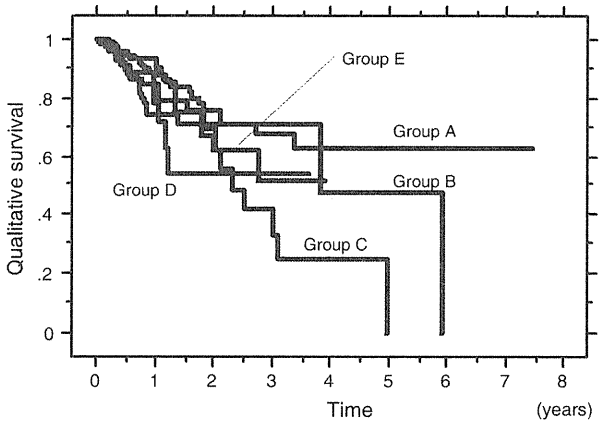

Fig. 5 Qualitative survival according to tumor number. The qualitative survival rate was 87.8% at 1 year and 73.0% at 2 years in all cases, and 90.7% in group A, 93.3% in group B, 80.8% in group C, 84.3% in group D, and 85.8% in group E. There were no significant differences between any two sequential groups

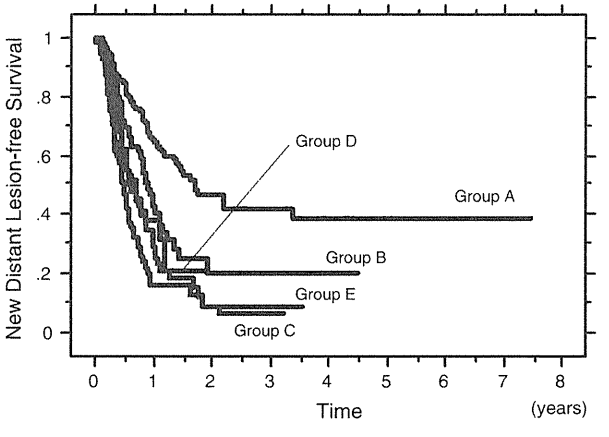

Fig. 6 New-lesion-free survival curves according to tumor number. The new-distant-lesion-free rate at 1 year was 54.3%. The new-distant-lesion-free rate at 1 year was 71.6% in group A, 53.7% in group B, 43.6% in group C, 50.7% in group D, and 66.3% in group E. There was significant difference between groups A and B ($p = 0.0003$) and also between groups B and C ($p = 0.0047$)

Discussion

Background of JLGK0901 study

The Japanese Radiation Oncology Study Group (JROSG) study reported by Aoyama [1] found no significant differences, in OS, NS or QS, between SRS alone and SRS with upfront WBRT, although new lesions and tumor progression were observed significantly more frequently with SRS alone. These results confirmed the efficacy of SRS alone for patients with 1–4 brain metastases. However, evidence supporting SRS alone for multiple brain tumors, i.e., exceeding 4, has not been established. Indeed, SRS using GK has been widely applied to multiple brain metastases, as reported especially by Japanese groups. Serizawa and Yamamoto [4–12] insisted that factors limiting SRS alone using GK include not only the number but also the size of lesions, presence of CSF dissemination, and total tumor volume. As the first step to filling the gap between broad clinical application and limited evidence for multiple brain tumors, we, the Japan Leksell Gamma Knife Society, planned a prospective multi-institute study of GK without upfront WBRT in selected patients with 1–10 brain metastases.

Introduction of JLGK0901 study

Based on the considerable experience and vast literature for GK alone in treating multiple brain metastases in Japan, the following intracranial conditions are not considered to be good indications for GK alone:

1. >10 cm^3 volume of the largest tumor
2. >15 cm^3 total tumor volume
3. Presence of CSF dissemination
4. Numerous (>10) brain metastases
5. Impaired ADL (<70 KPS) due to extracranial disease

Thus, the JLGK0901 study committee set the above as exclusion criteria. Cases with sarcoma, lymphoma, or cancer with unknown primary were also excluded. The protocol stipulates follow-up, including enhanced MRI and neurological examinations, at least every 3 months. Twelve hundred cases will be registered from 23 Japanese GK sites within 2 years, and a 1-year follow-up period will

be mandatory. This trial has been registered by the Japanese ethics committee (University Hospital Medical Information Network, UMIN 0000001812, http://www.umin.ac.jp/).

Expected results of the JLGK0901 study

In this retrospective study, all cases were eligible according to the inclusion criteria, and for the follow-up protocol, of the JLGK0901 study. Indeed, the results presented herein are attributable to our statistical base in the JLGK protocol. This prospective study is designed to prove the noninferiority of overall survival with several metastases in groups D and E versus 3–4 metastases in group C. With 80% statistical power, at the 0.025 level of probability (one sided), with a 2-year registration period, and 1-year follow-up after completion of registration, a planned total sample size of 1,200 has been determined for this prospective trial. Our experience leads us to conclude that the multiple brain metastases group (MST: 6.7 months) will not have results inferior to those of the oligo-brain metastases group (MST: 8.1 months) for 1-year survival with a noninferiority margin of 7.5% [13]. Noninferiority is confirmed if the upper limit of the confidence interval of the hazard ratio does not exceed the limit of 1.3, which is in accord with the noninferiority margin.

If our present retrospective results for patients with more than 4 brain metastases being almost the same as those of patients with 3–4 brain lesions are valid, the efficacy of GK alone for 5–10 brain metastases is anticipated to be confirmed by the JLGK0901 study, which is a well-designed prospective multi-institute controlled trial. If this study proves equality between 3–4, 5–6, and 7–10 brain metastases, in terms of OS, NS, QS, and NLFS, level 2 evidence of the efficacy of GK without prophylactic WBRT for multiple brain metastases will be established.

Conclusions

In terms of OS, NS, QS, and NLFS, GK without upfront WBRT for 1–10 brain metastases from various primary cancers provides excellent palliation considering the patients' short life expectancies. The results for patients with more than 4 brain metastases were almost the same as those of patients with 3–4 brain lesions in our retrospective study. These results are anticipated to be confirmed by the JLGK0901 study, which is a well-designed prospective multi-institute controlled trial. If this study proves equality between 3–4, 5–6, and 7–10 brain metastases in terms of OS, NS, QS, and NLFS, level 2 or 3 evidence of the efficacy of GK alone for 5–10 brain metastases will be established.

References

1. Aoyama H, Shirato H, Tago M, Nakagawara K, Toyoda T, Hatano Kenjo M, Oya N, Hirota S, Shioura H, Kunieda E, Inomata T, Hayakawa K, Katoh N, Kobayashi (2006) Stereotactic radiosurgery plus whole brain radiation therapy vs stereotactic radiosurgery alone for treatment of brain metastases: a randomized controlled trial. JAMA 295(21):20535–20536
2. Patchell RA, Tibbs PA, Walsh JW, Dempsey RJ, Maruyama Y, Kryscio RJ, Markesbery WR, Macdonald JS, Young B (1990) A randomized trial of surgery in the treatment of single metastases to the brain. N Engl J Med 322:494–500
3. Gaspar L, Scott C, Rotman M, Asbell S, Phillips T, Wasserman T, Mc Kenna WG, Byhardt R (1997) Recursive partitioning analysis (RPA) of prognostic factors in three Radiation Therapy Oncology Group (RTOG) brain metastases trials. Int J Radiat Oncol Biol Phys 37:745–751
4. Serizawa T, Iuchi T, Ono J, Saeki N, Osato K, Odaki M, Ushikubo O, Sato M, Matsuda S (2000) Gamma knife treatment for multiple metastatic brain tumors compared with whole-brain radiation therapy. J Neurosurg 93(Suppl 3):32–36
5. Serizawa T, Ono J, Iuchi T, Matsuda S, Sato M, Odaki M, Hirai S, Sato K, Yamaura A (2002) Gamma knife radiosurgery for metastatic brain tumors from lung cancer. Comparison between small cell cancer and non-small cell cancer. J Neurosurg 97(Suppl 5):484–488
6. Serizawa T, Saeki N, Higuchi Y, Ono J, Iuchi T, Nagano O, Yamaura A (2005) Gamma knife surgery for brain metastases: indications for and limitations of a local treatment protocol. Acta Neurochir (Wien) 147:721–726
7. Serizawa T, Higuchi Y, Ono J, Matsuda S, Iuchi T, Nagano O, Saeki N (2006) Gamma knife surgery for metastatic brain tumors from lung cancer without prophylactic whole brain radiation therapy. In: Kondziolka D (ed) Radiosurgery. Karger, Basel, Switzerland, pp 186–198
8. Serizawa T, Higuchi Y, Ono J, Matsuda S, Nagano O, Iwadate Y, Saeki N (2006) Gamma knife surgery for metastatic brain tumor without prophylactic whole brain radiation therapy: results in 1000 consecutive cases. J Neurosurg 105:86–90
9. Serizawa T, Yamamoto M, Nagano O, Higuchi Y, Matsuda S, Ono J, Iwadate Y, Saeki N (2008) Gamma knife surgery for metastatic brain tumors. A 2-institute study in Japan. J Neurosurg 109:118–121
10. Serizawa T (2008) Metastatic brain tumors: lung cancer. In: Yamamoto M (ed) Japanese experience with gamma knife radiosurgery. Karger, Basel, Switzerland, pp 142–153
11. Yang CC, Ting J, Wu X, Markoe A (1998) Dose volume histogram analysis of gamma knife radiosurgery treating twenty-five metastatic intracranial tumors. Stereotactic Funct Neurosurg 70:41–49
12. Yamamoto M, Ide M, Nishio S, Urakawa Y (2002) Gamma knife radiosurgery for numerous brain metastases: is this a safe treatment? Int J Radiat Oncol Biol Phys 53(5):1279–1283
13. Schoenfeld DA, Richter JR (1982) Nomograms for calculating the number of patients needed for a clinical trial with survival as an endpoint. Biometrics 38(1):163–170

Radiol Phys Technol (2010) 3:16–22
DOI 10.1007/s12194-009-0071-4

A parameter study of pencil beam proton dose distributions for the treatment of ocular melanoma utilizing spot scanning

Kenneth Sutherland · Satoshi Miyajima · Hiroyuki Date · Hiroki Shirato · Masayori Ishikawa · Masao Murakami · Mitsuru Yamagiwa · Paul Bolton · Toshiki Tajima

Received: 7 April 2009 / Revised: 4 August 2009 / Accepted: 4 August 2009 / Published online: 19 September 2009

Abstract The results of Monte Carlo calculated dose distributions of proton treatment of ocular melanoma are presented. An efficient spot scanning method utilizing active energy modulation, which also minimizes the number of target spots was developed. We simulated various parameter values for the particle energy spread and the pencil beam diameter in order to determine values suitable for medical treatment. We found that a 2.5-mm-diameter proton beam with a 5% Gaussian energy spread was suitable for treatment of ocular melanoma while preserving vision for the typical case that we simulated. The energy spectra and the required proton current were also calculated and are reported. The results are intended to serve as a guideline for a new class of low-cost, compact accelerators.

K. Sutherland (✉) · H. Date · H. Shirato · M. Ishikawa
Hokkaido University School of Medicine,
Kita-ku Kita 12 Jo Nishi 5 Chome,
Sapporo 060-0812, Japan
e-mail: kensuth@med.hokudai.ac.jp

K. Sutherland · S. Miyajima
Japan Science and Technology,
Motomachi 4 Chome 1 Ban 8 Go,
Kawaguchi, Saitama 332-0012, Japan

M. Yamagiwa · P. Bolton · T. Tajima
Photo-Medical Research Center, Japan Atomic Energy Agency,
Kizugawa, Kyoto 619-0215, Japan

M. Murakami
Hyogo Ion Beam Medical Center,
Shinguu Chou Hikarimiya 1-2-1,
Tatsuno, Hyogo, Japan

Keywords Proton therapy · Ocular melanoma · Monte Carlo simulation · Laser acceleration

1 Introduction

Proton beams have the potential to decrease normal tissue damage and allow dose escalation in cancer therapy, because the beam profile allows a more localized dose distribution at the tumor than do traditional X-rays. For covering the volume of a target lesion in particle therapy for cancer, two methods have been employed: passive scattering and spot scanning. In the passive scattering method, secondary neutrons from scatter foils, compensators and collimators are a possible source of secondary malignancy [1]. Spot scanning was first proposed as an alternative to passive scattering methods by Kanai et al. [2] and was further investigated by Lomax et al. [3]. Spot scanning utilizes magnetic and mechanical scanning of a pencil proton beam such that individually weighted Bragg peaks are distributed under computer control [4]. For spot scanning, there is no need for patient-specific collimators, thereby reducing the whole-body neutron dose to the patient. Another advantage is that most of the particles from the accelerator can be delivered to the patient, rather than being absorbed by collimators or compensators, and therefore this method is potentially more efficient.

In this work, we present the results of Monte Carlo simulations of proton dose distributions in which we used parameterized proton beams applied to ocular melanoma. We hope that the results of this study will serve as a guide for researchers developing proton facilities for medical treatment. We comment on the potential relevance of laser-accelerated protons [5–8] for the treatment of ocular melanoma, which requires lower proton energies than do more

deeply seated tumors, as well as relatively lower doses (fewer protons) because such tumors are typically small. However, the results should be applicable to proton therapy in general.

2 Materials and methods

2.1 Monte Carlo simulation speed improvements

Geant4 [9] version 8.0p1 was used for these simulations. Geant4 has been validated previously for medical-physics applications [10]. In order to improve the execution speed, we modified the particle navigation library following Jiang and Paganetti [11]. To improve efficiency on a PC cluster, we also developed a custom parallelization of Geant4 [12]. Simulations yield exactly the same results when running in parallel on a cluster or on a single processor as long as random-number-generator seed values are maintained and are set at the beginning of each event.

Following Jiang and Paganetti [11], four physics processes were registered in the Geant4 physics list for proton interactions: proton elastic scattering (*G4HadronElasticProcess*), proton inelastic scattering (*G4HadronInelasticProcess*), ionization (*G4hLowEnergyIonisation*) and multiple scattering (*G4MultipleScattering*). For improved efficiency, only secondary protons and neutrons were tracked. The energy from secondary electrons was deposited locally because the range was assumed to be less than 1 mm in water. The Geant4 maximum step size was limited to 1 mm.

2.2 Radiation treatment simulation software

We developed an application, which investigates the effects of the proton beam diameter and energy spread on the dose distribution. The software allows the user to open a series of DICOM CT images, and specify the target volume, one or more gantry positions and various beam characteristics. The user can also enter the particle (i.e., event) count. We chose a particle count of 1 million for this study, which we determined to be sufficient for good energy deposit distribution statistics with a reasonable processing time.

We used a series of 11 CT images of a disease-free human head with a slice thickness of 2.5 mm and a pixel spacing of 0.3125 mm. The CT pixel value (in Hounsfield units) of each voxel was used for determining the voxel material. Each material was assigned a density and a chemical composition according to the data provided by Schneider et al. [13]. The software generates files, which specify the different voxel materials and an event list containing the initial source position, direction and energy of each particle in the simulation. The dose accumulation grid had the same size and dimensions as the CT data: 512 × 512 × 11; i.e., we did not subsample or smoothen the CT values.

A database of depth and lateral dose profile curves was pre-computed with the use of the Monte Carlo package *Particle and Heavy Ion Transport Code System* (PHITS) [14, 15]. This database was used by our planning software for determining the initial energy peak, energy spread and spot spacing. Depth–dose curves were computed for proton beams incident on water with energies from 30 to 250 MeV in 1-MeV increments. Four values of the Gaussian energy spread were computed: 0, 5, 10 and 15%, at a depth resolution of 0.1 mm. Lateral offset tables were computed for energies from 30 to 200 MeV in 1-MeV increments, with the use of the same energy spread values, 0, 5, 10, and 15%, and with beam diameters of 0, 1.25, 2.5, 5 and 10 mm. The tables were stored in a binary format, which minimized the time necessary for reading of the data by the planning software.

An initial weighting factor was assigned to each target spot, which was used for determining the particle count. The deepest spot (associated with the highest energy) along a beam is assigned weight 1.0. Shallower spots are then assigned weights less than 1.0 based on the pre-computed database of dose distribution curves to achieve a spread-out Bragg peak (SOBP). The target weight is then used with the total particle count for assignment of individual particle counts for each target spot. At this step, the energy spread and beam diameter are factored in by addition of small random values to the initial energy and position of each particle. In the case of the energy spread, random numbers are chosen so that the resulting particle energies have a Gaussian distribution with the specified full width at half maximum (FWHM). Another pair of random numbers is chosen to place the particle within the specified beam diameter. Particles are distributed evenly along the beam axis. The particle list is then written on a file, which is read by the simulation program.

2.3 Target spot spacing

We incorporated a spot scanning method where the beam position and direction were fixed, while target spots along the beam direction were scanned by depth variation; i.e., active energy variation for depth modulation. All beams are assumed to be parallel to each other in this simulation (Fig. 1). This method requires a rapid alteration of the proton energy.

Our software also has the ability automatically to place target spots at locations with variable spacing based on the pre-computed database of dose profile curves in water. In the case of lateral spacing, lateral fall-off curves at the

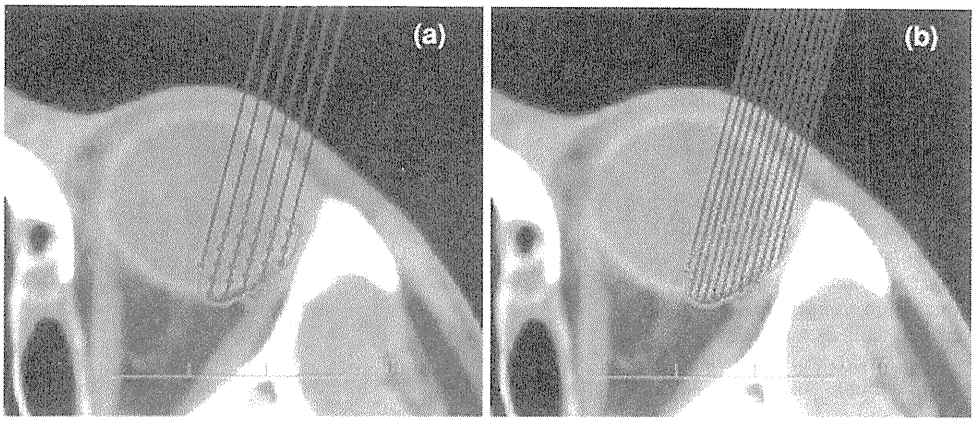

Fig. 1 Effect of beam parameters on target spot placement and beam spacing. *Blue lines* are beams. The *green polygon* is the planned target volume (PTV). *Red dots* are target spots. a 5-mm beam diameter and 10% energy spread. b 1.25-mm beam diameter and 0% energy spread, for which more target spots are generated (color figure online)

beam's pre-computed Bragg peak depth are used for determining the width (FWHM) of the beam, specifying a "spot width". The spot width is mostly affected by the beam diameter and by lateral scatter. For depth spacing, the beam's pre-computed depth–dose profile curve was used similarly for specifying a "spot depth". The spot depth is affected mostly by the energy spread.

Utilizing spot width and depth alone for spot spacing results in an uneven dose distribution within the target region due to under-dosed regions between spots. For achieving a smooth dose distribution, the spot width and the spot depth are multiplied by a "spacing factor". The spacing factor is usually less than 1.0 and has the effect of placing the spots closer together, i.e., increasing the number of spots. A spacing factor of 0.5, which we found yields a relatively smooth dose distribution while minimizing the number of target spots, was used throughout this simulation. A more detailed examination of the effect of the spacing factor on the dose distribution and the number of spots is a topic for future investigation.

2.4 Dose distribution optimization

It is difficult to predict the exact dose distribution in inhomogeneous patient volumes based on CT data alone. Therefore, after the initial Monte Carlo simulation, we fine-tuned the particle counts assigned to each target spot in the following way. The dose distribution for each target spot is calculated with the Monte Carlo simulation program and stored in separate files, one dose distribution file per target spot. The individual files are read and summed to form a complete dose distribution. The dose deposited at each target spot is compared with the dose average in the planning target volume (PTV). Spots that received less than the average dose (cold spots) are assigned more particles, and spots with a higher dose (hot spots) are assigned fewer particles. The process is repeated iteratively until it is determined that the result cannot be optimized further. Note that we do not attempt to reduce the dose deposited in critical structures; we only attempt to achieve a uniform dose distribution within the target volume in this optimization process.

2.5 Target polygon

The gross target volume (GTV) was modeled as a semi-ellipsoid with a semi-sphere base of height 4.8 mm and basal diameter 13 mm. The minimum tumor–optic disk distance was 5 mm. The tumor–macula distance was 4 mm. The values were chosen to represent a typical tumor based on data reported by Dendale et al. [16]. The GTV was generated in the planning software by specification of the tumor height, base diameter, eye center and tumor base position. A 2-mm margin was automatically added to the perimeter of the GTV to form the PTV. The volume of the PTV was .734 cm^3. The target polygon (PTV) and organs at risk (OARs) are shown in Fig. 2.

The prescribed dose was set to 54.5 Gy, which is equal to 60 cobalt Gray equivalent (CGE), assuming a relative radiobiological effectiveness (RBE) of 1.1. The tumor was assumed to be free of infiltration of the optic disk or macula. The dose distribution was normalized so that ninety-five percent of the PTV received at least 100% of the prescribed dose; i.e., "D95" for the PTV was set to 60 CGE. Four fractions in one week were assumed to be used, which is the common practice in conventional proton therapy. The effects of the energy spread and beam diameter were investigated with 60 CGE kept for D95 in each calculation.

3 Results

In the first series of simulations, the effect of the energy spread of the beam on the dose distribution was investigated. Energy spread values of 5, 10 and 15% were simulated. The beam diameter was 2.5 mm in each case. Dose distributions are shown in Fig. 3. Dose–volume

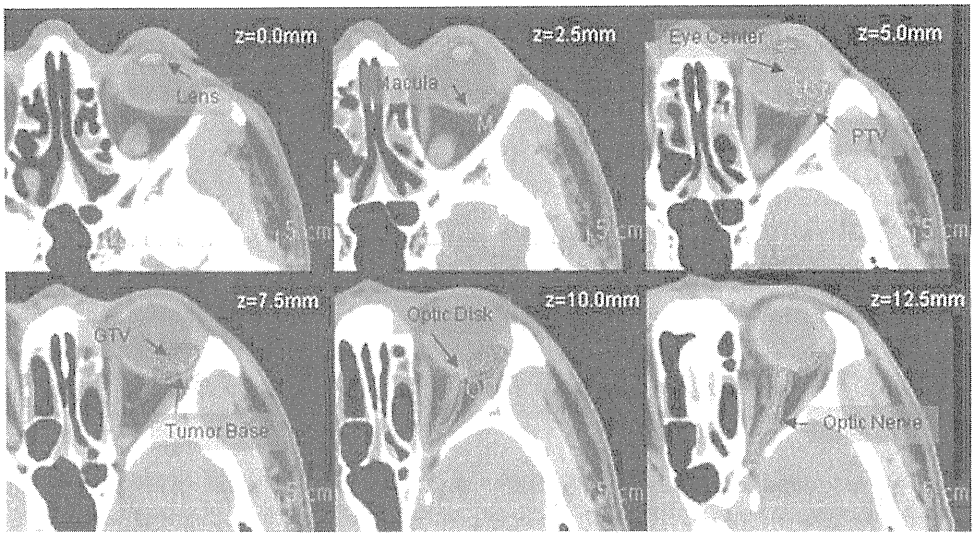

Fig. 2 Target polygons and organs at risk (OARs) used for this experiment. The inner target polygon is the *GTV*. The GTV is generated automatically by specifying the location of the tumor base and eye center. The size of the GTV is determined by specifying the basal diameter and tumor height. The outer target polygon is the *PTV* (GTV plus 2-mm margin). OARs include the lens, optic nerve macula, and optic disk (color figure online)

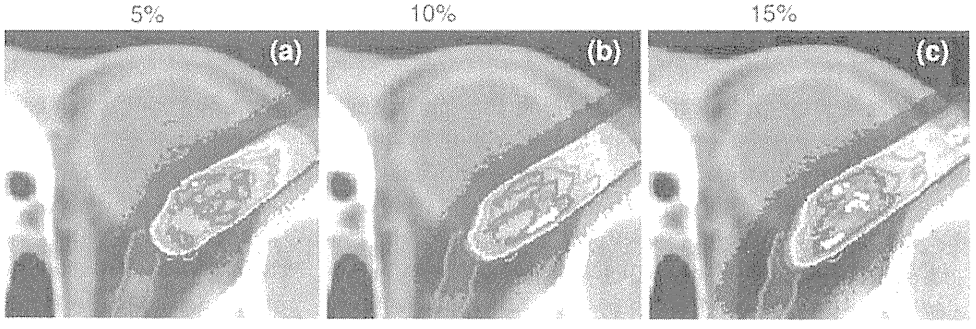

Fig. 3 Dose distributions for various values of energy spread. 5% (**a**), 10% (**b**) and 15% (**c**). Isodose lines are 125% of prescribed dose (75 CGE) *white*, 110% (66 CGE) *red*, 90% (54 CGE) *orange*, 75% (45 CGE) *yellow*, and 50% (30 CGE) *blue*. In all cases, a 2.5-mm beam width was used (color figure online)

histograms (DVHs) are shown in Fig. 4, and simulation results are summarized in Table 1. The table indicates that, at 5% energy spread, the dose to the macula and optic disc was below the tolerance values for the case that we simulated. At 10 and 15%, it was difficult to preserve critical structures located behind the distal edge of the target volume due to the elongated fall-off of the depth profile curve.

Target spot and beam characteristics are summarized in Table 2. The table shows the effect of energy spread (5, 10 and 15%) on the depth spacing and the number of target spots with a constant beam diameter (2.5 mm). The depth spacing (the distance between target spots along a beam) is increased with increasing energy spread, whereas the number of target spots is decreased with increasing energy spread.

In the second series, the effect of the beam diameter on the dose distribution was investigated. Beam diameter values of 1.25, 2.5 and 5 mm were simulated. The energy spread value for each case was 5%. Dose distributions are shown in Fig. 5, and DVHs are shown in Fig. 6. Figure 5 illustrates that the volume of hot spots in the PTV increased when the beam diameter was increased from 1.25to 2.5 mm. The simulation results are summarized in Table 3.

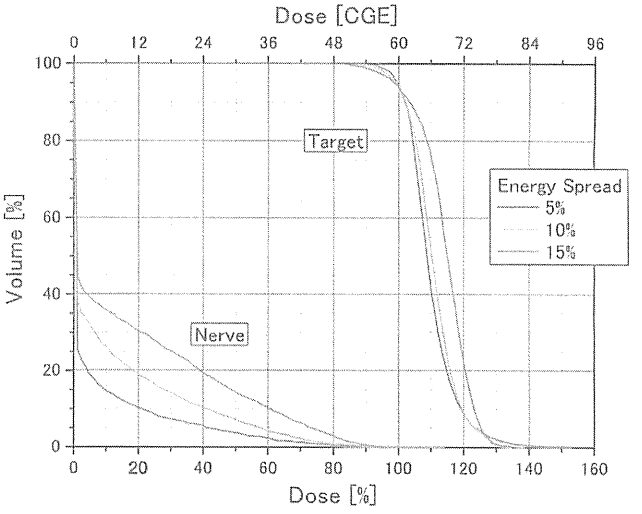

Fig. 4 DVH of PTV and optic nerve for various energy spread values. In all cases a 2.5-mm beam diameter was used (color figure online)

The table indicates that a beam diameter of less than or equal to 2.5 mm would not exceed the tolerance doses for the case that we studied. At 5-mm beam diameter, the dose to the lens becomes significant.

Table 4 indicates the effect of the beam diameter (1.25, 2.5 and 5 mm) with a fixed energy spread of 5%. The maximum and minimum values of the depth spacing were almost constant, as anticipated from the fixed energy spread. Also, the beam diameter affected the lateral spacing, as expected. The number of beams and target spots decreased significantly with an increase in the beam diameter. For a beam of 1.25 mm, nearly a thousand target spots were generated by the planning software. Such a large number of target spots would likely require a lot of time to treat.

A histogram of particle energy for a typical treatment plan is displayed in Fig. 7. In general, more particles at the higher-energy end of the spectrum are necessary because more particles are targeted at deeper locations in forming the SOBP. The energy distribution is also affected by the target shape and the incident beam direction. The energy distribution is not smooth, partly due to the discrete proton energy values used for our calculations.

Table 1 Dosimetric characteristics: energy spread

Energy spread	5%	10%	15%
Retina ≥45 CGE	1%	2%	5%
Lens ≥10 CGE	0%	0%	0%
Optic nerve ≥12 CGE	10%	20%	31%
Dose at macula (≥30 CGE)	27 (OK)	36 (NG)	42 (NG)
Dose at optic disc (≥12 CGE)	11 (OK)	1.8 (OK)	3.3 (OK)
V95[a]	98%	98%	97%

[a] Percentage volume of PTV, which received 95% of the prescribed dose (57 CGE)

Table 2 Target spot and beam characteristics: energy spread

Energy spread	5%	10%	15%
Lateral spacing (mm)	1.3	1.3	1.3
Depth spacing, minimum (mm)	0.6	1.7	3.1
Depth spacing, maximum (mm)	2.8	5.8	9.1
Number of beams	38	38	38
Number of target spots	239	102	65

Beamlet diameter was 2.5 mm for each case

4 Discussion

Many parameters and parameter combinations (such as beam diameter, energy spread, lateral spacing, depth spacing, number of beams and number of target spots) must be considered in assessing proton treatment of small superficial tumors. Realistically, some of the parameters may need to be predetermined in the clinical equipment because of mechanical or other limitations. In this study, we simulated the effect of energy spread by using a fixed beam diameter (2.5 mm), and the effect of the beam diameter by using a fixed energy spread (5%). These values were chosen because they seemed to be the most likely parameters delivered by an actual accelerator. A more thorough parameter survey is necessary for determination of the effects of every possible combination of beam parameters.

For reducing treatment times, it is desirable to reduce the number of target spots in a plan. However, there is a trade-off between the dose distribution and the number of target spots. Our results suggest that, if the beam energy and lateral spacing are predetermined, the energy spread and beam diameters must be chosen carefully with this in mind. The clinical significance of dose–volume statistics of the PTV and organs at risk must be determined for each patient.

The dose distributions shown here contain many hot spots (overdose areas). These are caused partially by the histogram normalization method, where 95% of the target volume is forced to receive at least 100% of the prescribed dose. Without normalization, cold spots were prevalent around the lateral and distal edges, especially when a large beam diameter or energy spread was used. The cold spots became prevalent when the distance from the tumor polygon edge and nearest target spot was relatively large. This resulted in DVH curves for the target volume not being as steep (selective) as they should have been. Several methods can be employed for improving the dose distributions,

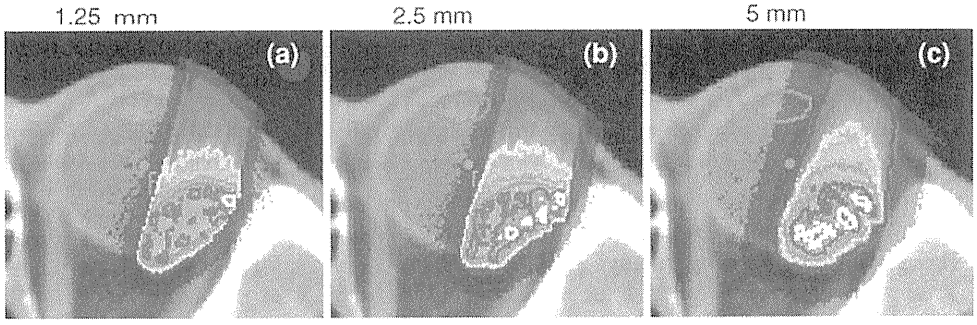

Fig. 5 Dose distribution for various values for beam diameter, 1.25 mm (**a**) 2.5 mm (**b**), and 5 mm (**c**). Isodose lines are 125% of prescribed dose (75 CGE) *white*, 110% (66 CGE) *red*, 90% (54 CGE) *orange*, 75% (45 CGE) *yellow* and 50% (30 CGE) *blue*. In all cases, we used 5% energy spread (color figure online)

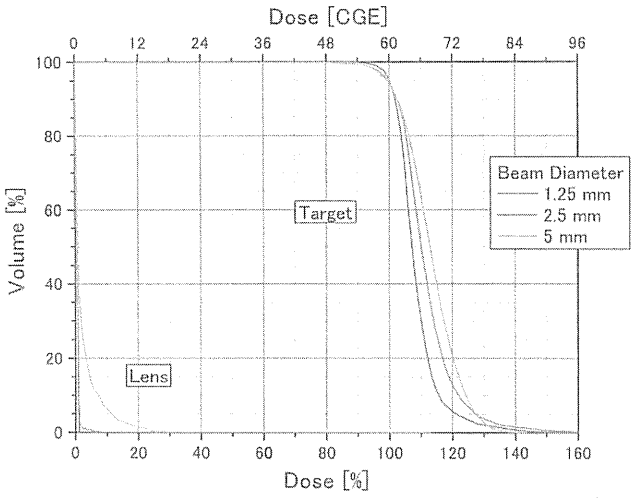

Fig. 6 DVH for PTV and optic nerve computed with various values for beam diameter. In all cases, we used 5% energy spread (color figure online)

Table 3 Dosimetric characteristics: beam diameter

Beam diameter	1.25 mm	2.5 mm	5 mm
Retina ≥45 CGE	0%	0%	1%
Lens ≥10 CGE	0%	0%	6%
Optic nerve ≥12 CGE	0%	1%	4%
Dose at macula (≥30 CGE)	13 (OK)	13 (OK)	36 (NG)
Dose at optic disc (≥12 CGE)	0.8 (OK)	3.0 (OK)	18 (NG)
V95[a]	99%	98%	98%

[a] Percentage volume of CTV, which received 95% of the prescribed dose (57 CGE)

Table 4 Spot and beam characteristics: beam diameter

Beam diameter	1.25 mm	2.5 mm	5 mm
Lateral spacing (mm)	0.7	1.4	2.6
Depth spacing, minimum (mm)	0.7	0.7	0.6
Depth spacing, maximum (mm)	2.4	2.4	2.3
Number of beams	206	57	21
Number of target spots	918	233	87

Energy spread was 5% for each case

including increasing the number of Monte Carlo events, decreasing the space between target spots and improving the optimization algorithm. Furthermore, we used a fixed spacing factor of 0.5 in this study. Introduction of a variable spacing factor for each beam may further improve the homogeneity of dose distributions. The spacing factor should be smaller near the polygon edges to prevent cold spots while maintaining a reasonable total number of spots. These are topics for future study.

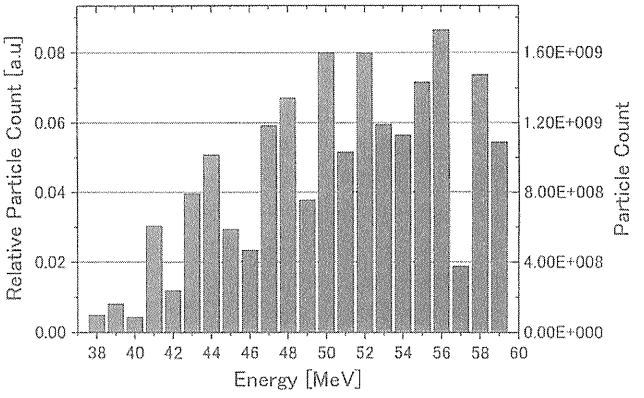

Fig. 7 A typical histogram of particle energy levels (color figure online)

In this work, doses to the macula and to the optic disc were high and above the clinical limits in some cases. This is mainly because these structures are located directly behind the distal edge of the target volume. Proton spectra that are closer to being monoenergetic may improve the final clinical outcome. The effect of energy spread for deep-seated tumors such as prostate cancer may be different from that for shallow ocular diseases and is yet to be determined.

The required proton flux can be estimated as follows. Consider a shallow tumor volume of 1 cc (1 g). If the protons deposit an average energy of 50 MeV, then each proton delivers about 8×10^{-12} J or 8×10^{-9} Gy on average. Assuming an RBE of 1.1, each proton delivers about 9×10^{-9} CGE. A typical treatment course consists of 60 CGE delivered in four fractions on consecutive days. If the irradiation time is limited to 1 min, then the accelerator must deliver 15 CGE per min or .25 CGE per s. The accelerator must therefore produce about 30 million protons per second or 4.8 pA. If such a delivery was carried out in 100 Hz repetitive pulsed laser shots, the required delivery would be in the order of 3×10^5 protons per shot.

5 Conclusion

Our simulations show that a 2.5-mm beam diameter and a 5% energy spread can be considered as a starting point for ocular cases. The dose distributions suggest that there is merit in continuing such parameter studies and considering further the potential for spot scanning proton sources.

Acknowledgments This work was supported by the Core Research for Evolutional Science and Technology (CREST), the Japan Science and Technology Agency (JST) and the Special Coordination Fund (SCF) for Promoting Science and Technology commissioned by the Ministry of Education, Culture, Sports, Science and Technology (MEXT) of Japan. K. S. is a Takuma Scholar of PMRC.

References

1. Brenner DJ, Hall EJ. Secondary neutrons in clinical proton radiotherapy: a charged issue. Radiat Oncol. 2008;86(2):165–70.
2. Kanai T, Kawachi K, Kumamoto Y, Ogawa H, Yamada Y, Matsuzawa H. Spot scanning system for proton radiotherapy. Med Phys. 1980;7(4):365–9.
3. Lomax AJ, Bohringer T, Bolsi A, Coray D, Emert F, Goitein G, et al. Treatment planning and verification of proton therapy using spot scanning: initial experiences. Med Phys. 2004;31(11):3150–7.
4. Lomax AJ, Boehringer T, Coray A, Egger E, Goitein G, Grossmann M, et al. Intensity-modulated proton therapy: a clinical example. Med Phys. 2000;28(3):317–24.
5. Tajima T. Prospect for compact medical laser accelerators. J Jpn Soc Therap Radiat Oncol. 1997;9(Suppl 2):83–5.
6. Malka V, Sven F, Lefebvre E, d'Humieres E, Ferrand R. Practicability of proton therapy using compact laser systems. Med Phys. 2004;31(6):1587–92.
7. Ma CM, Maughan RL. Point/counterpoint: within the next decade conventional cyclotrons for proton radiotherapy will become obsolete and replaced by far less expensive machines using compact laser systems for the acceleration of the protons. Med Phys. 2006;33(3):571–3.
8. Bulanov SV, Esirkepov T, Khoroshkov VS, Kuznetsov AV, Pegoraro F. Oncological hadrontherapy with laser ion accelerators. Phys Lett A. 2002;299:240–7.
9. Agostinelli S, Allisonas J, Amakoe K, Apostolakisa J, Araujo H, et al. Geant4–a simulation toolkit. Nucl Instrum Methods Phys Res A. 2003;506:250–303.
10. Carrier J, Archambault L, Beaulieu L, Roy R. Validation of Geant4, an object-oriented Monte Carlo toolkit, for simulations in medical physics. Med Phys. 2004;31(3):484–92.
11. Jiang H, Paganetti H. Adaptation of Geant4 to Monte Carlo dose calculations based on CT data. Med Phys. 2004;31(10):2811–8.
12. Sutherland K, Miyajima S, Date H. A simple parallelization of Geant4 on a PC cluster with static scheduling for dose calculations. First European workshop on Monte Carlo treatment planning, Journal of Physics: Conference Series. 2007; 74 012020.
13. Schneider W, Bortfeld T, Schlegel W. Correlation between CT numbers and tissue parameters needed for Monte Carlo simulations of clinical dose distributions. Phys Med Biol. 2000;45:459–78.
14. Iwase H, Niita K, Nakamura T. Development of a general-purpose particle and heavy ion transport Monte Carlo code. J Nucl Sci Technol. 2002;39(11):1142–51.
15. Niita K, Sato T, Iwase H, Nose H, Nakashima H, Sihver L. PHITS: a particle and heavy ion transport code system. Radiat Meas. 2006;41:1080–90.
16. Dendale R, et al. Proton beam radiotherapy for uveal melanoma: results of Curie Institute-Orsay Proton Therapy Center (ICPO). Int J Radiat Oncol Biol Phys. 2006;65(3):780–7.

JJCO Japanese Journal of Clinical Oncology

Jpn J Clin Oncol 2010;40(8)788–794
doi:10.1093/jjco/hyq044
Advance Access Publication 20 April 2010

Clinical Outcomes of Stereotactic Brain and/or Body Radiotherapy for Patients with Oligometastatic Lesions

Tetsuya Inoue[1,*], Norio Katoh[1], Hidefumi Aoyama[1], Rikiya Onimaru[1], Hiroshi Taguchi[1], Shunsuke Onodera[1], Satoshi Yamaguchi[2] and Hiroki Shirato[1]

[1]Department of Radiology, Hokkaido University Graduate School of Medicine and [2]Department of Medical Physics, Hokkaido University Graduate School of Medicine, Sapporo, Japan

*For reprints and all correspondence: Tetsuya Inoue, Department of Radiology, Hokkaido University Graduate School of Medicine, North 15 West 7, Kita-ku, Sapporo 060-8638, Japan. E-mail: t-inoue@med.hokudai.ac.jp

Received November 30, 2009; accepted March 11, 2010

Objective: Several recent studies have shown that oligometastatic disease has curative potential, although it was previously considered to signal a patient's last stage of life. Stereotactic body radiotherapy has been available for extra-cranial metastases in addition to stereotactic cranial radiotherapy for brain metastases. The aim of the present study was to retrospectively evaluate the clinical outcomes of stereotactic radiotherapy for patients with oligometastatic lesions.

Methods: Between 1999 and 2008, 41 patients with five or fewer detectable metastases were treated with stereotactic radiotherapy at our institution. The treated oligometastatic lesions were in the brain, lung and adrenal glands.

Results: With a median follow-up period of 20 months, the 3-year overall survival, progression-free survival, local control and distant control rates were 39%, 20%, 80% and 35%, respectively, and the respective 5-year rates were 28%, 20%, 80% and 35%. The median survival time was 24 months. According to interval to recurrence, the 3- and 5-year overall survival rates were 19% and 10%, respectively, for patients with <12 months ($n=18$), compared with 53% and 40% for those with ≥ 12 months ($n=23$) ($P=0.006$).

Conclusions: Precise stereotactic radiotherapy was effective in controlling oligometastatic lesions for patients with a median survival time of 24 months. Interval to recurrence may impact the overall survival rate and should be included in the stratification criteria in a prospective randomized trial to investigate the benefits of stereotactic radiotherapy for patients with oligometastases.

Key words: oligometastases – stereotactic body radiotherapy – stereotactic radiotherapy – radiosurgery

INTRODUCTION

Most patients who have had any recurrent or metastatic sites of cancer are considered to be in their last stage of life. However, stereotactic cranial radiosurgery (SCRS) and stereotactic cranial radiotherapy (SCRT) have been shown to be useful for prolonging useful life in patients with solitary or oligo brain metastases with or without whole brain radiotherapy (WBRT) (1,2). The treatment outcomes are related to the number of metastases and the presence or absence of extra-cranial disease (3). A Phase III study has suggested that SCRS with WBRT results in better survival than WBRT alone for patients with a single brain metastasis or patients with tumors > 2.0 cm in diameter (4). These studies have shed light on the possibility of improving treatment outcomes by using high-dose local radiotherapy with or without whole-body cancer treatment in patients with extra-cranial metastasis.

Stereotactic body radiotherapy (SBRT) with high local dose has been applied to extra-cranial diseases such as peripheral Stage I non-small cell lung cancer (NSCLC) and has been reported to provide excellent local control (LC) and survival compatible with surgery (5,6). Recently, indications for SBRT have been extended to include lung metastases (7–9), liver metastases (10,11), adrenal gland metastases (12,13), spinal metastases (14–16), and others (17). Excellent LC has been reported in these reports, but the clinical benefits of SBRT for extra-cranial metastasis are yet to be determined. In most of these studies, SBRT was used for patients with fewer than five metastatic sites or for those in the clinical state of so-called oligometastasis (18).

The clinical state of oligometastatic disease was proposed in 1995 by Hellman and Weichselbaum (18), who hypothesized that LC of oligometastases may yield improved systemic control and prolonged survival. Niibe et al. (19–21) have also reported the state of oligometastasis/oligo-recurrence. They suggested that some oligometastasis/oligo-recurrence patients could survive for as long as the patients with primary cancer only, and thus these patients must be treated curatively. Improvements in diagnostic modalities have facilitated early detection of small metastatic lesions, both intra-cranial and extra-cranial, and have provided a sound rationale for Hellman and Weichselbaum's hypothesis. Recent clinical research has shown that some patients with recurrence or distant metastases can expect long-term survival after SBRT and SCRT (7–11,19–23). It remains uncertain whether these results are due to selection bias or some positive effect of SBRT and SCRT. A prospective randomized trial should be undertaken to answer this question, but prognostic factors to stratify the patients are not yet well understood.

In this study, we retrospectively analyzed our experience with SBRT and/or SCRT/SCRS for patients with oligometastases.

PATIENTS AND METHODS

Patient Characteristics

A database of patients who received SBRT and SCRT/SCRS at our institution was used to select the patients whose primary sites were treated by surgery or definitive radiation therapy between 1995 and 2007. There were 41 patients who had five or fewer detectable oligometastatic lesions at the time of SBRT and/or SCRT and had been treated with SBRT and/or SCRT/SCRS between 1999 and 2008. Diagnosis of the oligometastatic lesions was based on whole-body computed tomography (CT) and brain magnetic resonance imaging (MRI) findings. Fluorodeoxyglucose-positron emission tomography was performed as needed. The oligometastatic lesions were diagnosed by diagnostic radiologists during the diagnostic evaluation.

The treatment methods for the primary sites were surgery in 23 patients and definitive radiotherapy in 18. Definitive radiotherapy consisted of conventional radiotherapy in 8 patients and SBRT in 10.

There were seven patients who had previously been treated by SBRT and/or SCRT/SCRS to oligometastatic sites prior to receiving surgery or radiotherapy at their primary sites. The treatment time interval between the surgery/definitive radiation therapy to the primary sites and the initial SBRT and/or SCRT/SCRS to oligometastatic sites ranged from 1 to 4 months (median 2 months) in these seven patients. In the other 34 patients, the median treatment interval time from primary sites to oligometastatic sites was 21 months (range 0–121 months). We defined the treatment interval time from primary sites to oligometastatic sites as interval to recurrence. In this study, all analyses started from the day of SBRT and/or SCRT/SCRS to oligometastatic sites.

The patient characteristics are given in Table 1. There were 22 men and 19 women, and the median age was 66 years (range 30–82 years). The primary cancers consisted of lung cancer, head and neck cancer, breast cancer, colorectal cancer, renal cell carcinoma, renal pelvic cancer, hepatocellular carcinoma, thymic cancer and apocrine gland cancer. The study patients were separated into a favorable group (breast, colorectal, renal, thymic and apocrine gland cancer) and others, according to Rusthoven et al. (10). The primary histology was mainly adenocarcinoma. The number of oligometastatic tumors was mainly one or two tumors; there were only two patients who had three oligometastatic tumors and only one patient who had five. The sites involved with the oligometastatic lesions were the brain, lung and adrenal gland. Lung and adrenal gland metastases were treated by SBRT. There were no patients with oligometastatic liver metastases treated by SBRT at our institution. Fourteen patients were treated by chemotherapy as an adjuvant therapy or as a treatment for recurrence or metastases. No chemotherapy was administered during the treatment for oligometastases. No patients underwent surgical removal of the metastatic lesions.

There were 24 patients who had single or multiple brain metastases. Brain metastases were treated by SCRT or SCRS. According to the recursive partitioning analysis, 5, 18 and 1 patients were classified as Class I, Class II and Class III, respectively.

SCRT/SCRS Technique

Fifteen of 24 patients were treated by SCRT alone, five by SCRS alone and four by SCRS with WBRT for their brain metastases. The patients who received WBRT were randomly assigned to the group of SCRS with WBRT by the clinical trial of the Japanese Radiation Oncology Study Group (JROSG 99-1) (2). These patients were treated with 6- or 10-MV photons using a linac-based stereotactic system and were immobilized by a thermoshell in SCRT and a stereotactic frame in SCRS. The gross tumor volume (GTV) was defined based on MRI and CT images. A 1–3-mm